

Dehydration of 4-methylpentan-2-ol over $Ce_xZr_{1-x}O_2/SiO_2$ nano-composite catalyst

Benjaram M. Reddy*, Pandian Lakshmanan, Pankaj Bharali, Pranjal Saikia

Inorganic and Physical Chemistry Division, Indian Institute of Chemical Technology, Hyderabad 500007, India

Received 23 June 2006; accepted 16 July 2006

Available online 24 August 2006

Abstract

Surface stabilized nano-sized ceria–zirconia solid solution on silica support was synthesized through a soft chemical route using colloidal silica dispersion and nitrate precursors of cerium and zirconium. The dispersion and structural stability of the $Ce_xZr_{1-x}O_2$ solid solution after thermal treatments at 773 and 1073 K was investigated by means of X-ray diffraction (XRD), high-resolution transmission electron microscopy (HREM), X-ray photoelectron spectroscopy (XPS) and BET surface area techniques. Catalytic performance of the synthesized $Ce_xZr_{1-x}O_2/SiO_2$ sample was tested for the conversion of 4-methylpentan-2-ol to 4-methylpent-1-ene in the vapour phase under normal atmospheric pressure. From XRD measurements, the presence of cubic phases of the composition $Ce_{0.75}Zr_{0.25}O_2$, $Ce_{0.6}Zr_{0.4}O_2$ and $Ce_{0.5}Zr_{0.5}O_2$ were identified. The former phase was noted at 773 K and the later phases at 1073 K indicating enrichment of zirconium in the cubic fluorite type ceria lattice at higher calcination temperature. HREM results revealed existence of very small Ce–Zr mixed oxide crystallites of ~ 5 nm size over amorphous silica at 773 K. No appreciable increase in the size of the crystallites was noticed even after calcination at 1073 K. XPS measurements indicated significant amount of Ce^{3+} present in the samples. All the characterization techniques revealed that silica does not form any unwanted inert compounds with the dispersed Ce–Zr-oxides. The activity studies reveal that the $Ce_xZr_{1-x}O_2/SiO_2$ catalyst exhibits a high and stable activity in the time-on-stream experiments with good product selectivity to 4-methylpent-1-ene. Also a significant decrease in the reaction temperature corresponding to 50% conversion is noted over this catalyst.

© 2006 Elsevier B.V. All rights reserved.

Keywords: Ceria–zirconia; Solid solution; $Ce_xZr_{1-x}O_2/SiO_2$; XRD; HREM; XPS; 4-Methylpentan-2-ol; 4-Methylpent-1-ene

1. Introduction

Cerium dioxide, the most studied oxide material among all the rare earth elements has received tremendous research interest recently due to its application in various fields including catalysis and materials science [1,2]. The most important property that makes the ceria remarkable is its oxygen storage and release capacity via the redox shift between Ce^{4+} and Ce^{3+} under oxidizing and reducing conditions, respectively. Therefore, ceria containing oxides have been profitably employed in the automotive pollution abatement three-way catalytic converters (TWC). Pure ceria alone exhibits poor thermal stability and susceptible to sintering at high temperatures leading to catalyst deactivation

[3]. Therefore, several CeO_2 -based mixed oxide systems have been investigated to overcome the disadvantages associated with the unsupported cerium oxide [4]. Ceria easily forms solid solutions with transition metals and other rare-earth elements. It has been established that introduction of zirconium into the ceria lattice greatly enhances the surface area, thermal stability and oxygen storage capacity resulting superior catalytic properties. Hence, ceria–zirconia solid solutions have been investigated with huge interest among other ceria-based mixed oxides [5–7]. Typical catalytic applications of these oxides include partial oxidation of methane to generate hydrogen for fuel cell applications [9], CO_2 reforming of methane to produce synthesis gas [10], direct oxidation of methane in the solid oxide fuel cells (SOFC) [11], steam reforming of ethanol [12] and hydrodesulfurization sorbents [13].

The conversion of 4-methylpentan-2-ol to 4-methylpent-1-ene is an important reaction from the practical viewpoint as an alternative route to the production of 4-methylpent-1-ene,

* Corresponding author. Tel.: +91 40 2716 0123; fax: +91 40 2716 0921.

E-mail addresses: bmreddy@iict.res.in, mreddyb@yahoo.com (B.M. Reddy).

a monomer for the manufacture of thermoplastic polymers of superior technological properties. Unsupported forms of $Ce_xZr_{1-x}O_2$ solid solutions have been employed for this reaction [14,15]. It was observed that the CeO_2 - ZrO_2 catalysts exhibit good catalytic activity and the acid–base character of the catalyst is most important in order to obtain high selectivity to the desired 1-alkene and to avoid the formation of olefins with internal double bonds and the dehydrogenation product ketone. Despite their wide applicability for various reactions, the unsupported forms of $Ce_xZr_{1-x}O_2$ solid solutions are known to suffer from typical disadvantages such as low specific surface area, low thermal resistance to sintering and low structural/textural stability during high temperature applications [8]. The present investigation was undertaken to overcome the deficiencies of the $Ce_xZr_{1-x}O_2$ solid solutions and explore them for various catalytic applications. In this study, a high surface area and stable $Ce_xZr_{1-x}O_2/SiO_2$ nano-composite catalyst (CZ/S) was synthesized via a deposition precipitation technique employing aqueous colloidal silica dispersions. The synthesized catalyst, calcined at various temperatures, was characterized using XRD, HREM, XPS and BET surface area techniques, and evaluated for its catalytic performance towards the dehydration of 4-methylpentan-2-ol to 4-methylpent-1-ene in the vapour phase under normal atmospheric pressure. An attempt was also made to correlate the enhanced reactivity with the structural features of this catalyst.

2. Experimental

2.1. Catalyst preparation

The CeO_2 - ZrO_2/SiO_2 catalyst (1:1:2 mole ratio based on oxides) was synthesized by a deposition precipitation method. Nitrate precursors, ammonium cerium(IV) nitrate (Loba Chemie, GR grade) and zirconium(IV) nitrate (Fluka, AR grade) in requisite quantities were dissolved separately in deionized water and mixed together. To the aforementioned mixture solution, required quantity of colloidal silica (Ludox 40 wt.%, Aldrich, AR grade) was added under vigorous stirring. Dilute aqueous ammonia solution was added dropwise with vigorous stirring until the precipitation was complete (pH 8.5). The resulting product was filtered off, washed several times with deionized water, oven dried at 383 K for 12 h, and then calcined at 773 K for 5 h in air atmosphere. Some portions of the finished sample were once again heated at 1073 K for 5 h in air atmosphere in order to study the structural/textural stability of the catalyst.

2.2. Characterization

The X-ray powder diffraction (XRD) patterns were obtained with a Siemens D500 diffractometer using Ni-filtered $Cu K\alpha$ radiation. Crystalline phases in the samples were identified by matching experimental patterns with the PDF-ICDD files. The mean crystallite size was estimated by applying Scherrer equation. The 'a' cell parameter was calculated by a standard cubic indexing method, using the intensity of the base peak (1 1 1) [16]. X-ray photoelectron spectroscopy (XPS) was performed

using Shimadzu (ESCA 3400) spectrometer equipped with $Mg K\alpha$ (1253.6 eV) source. Charging of the samples was corrected by setting the binding energy of adventitious carbon (C 1s) at 284.6 eV [17]. The XPS analysis was done at ambient temperature and pressures typically below 10^{-6} Pa. The BET surface area measurements were made using a Gemini 2360 instrument. Prior to analysis, samples were degassed at 393 K under vacuum for 8 h to remove residual moisture and other volatiles. HREM investigations were performed using a Philips CM200 electron microscope with 0.23 nm point-to-point resolution. The samples were supported on a holey carbon copper grid by dropping ethanol suspensions containing the uniformly dispersed oxide powders.

2.3. Catalytic activity

The dehydration of 4-methylpentan-2-ol was investigated in the vapour phase under normal atmospheric pressure, in a down flow fixed bed micro-reactor, at different temperatures. In a typical experiment ca. 0.5 g of catalyst sample was secured between two plugs of quartz wool inside the quartz micro-reactor (i.d. 0.8 cm) and above the catalyst bed filled with ceramic beads in order to act as preheating zone. The reactor was placed vertically inside a tubular furnace, which can be heated electrically. The reactor temperature was monitored by a thermocouple with its tip located near the catalyst bed and connected to a temperature indicator-controller. Prior to the reaction, the catalyst was preheated at 773 K for 6 h under CO_2 -free airflow. The 4-methylpentan-2-ol was fed with N_2 stream, with the time factor $0.5 \text{ g}_{\text{catalyst}}/\text{g}_{\text{alcohol}}$. The condensed liquid products were analysed qualitatively by NMR and MS techniques and quantitatively by gas chromatography. The conversion and selectivity were calculated as per the procedure described elsewhere [18].

3. Results and discussion

The powder XRD patterns of CZ/S sample calcined at 773 and 1073 K are shown in Fig. 1. As can be noted from this figure, sample calcined at 773 K exhibits poor crystallinity. Only broad diffraction lines due to the cubic fluorite type phase with the composition $Ce_{0.75}Zr_{0.25}O_2$ (PDF-ICDD 28-0271) could be identified. With increase of calcination temperature from 773 to 1073 K, there is an upward shift in the peak positions and the lines due to the presence of $Ce_{0.6}Zr_{0.4}O_2$ (PDF-ICDD 38-1439) and $Ce_{0.5}Zr_{0.5}O_2$ (PDF-ICDD 38-1436) phases could be inferred indicating incorporation of more zirconium into the cerium oxide unit cell at higher calcination temperature. This observation is further supported by a decrease in the cell 'a' parameter value from 5.35 to 5.26 Å with increasing calcination temperature from 773 to 1073 K (Table 1). According to Vegard's law, a decrease of lattice parameter or cell volume is expected due to insertion of more quantity of Zr^{4+} into the CeO_2 lattice, since the ionic radius of Zr^{4+} (0.084 nm) is smaller than that of Ce^{4+} (0.097 nm) [16]. There is no evidence for the formation of *t*- ZrO_2 or *m*- ZrO_2 phases of zirconia within the detection limits of the XRD technique. Additionally, the XRD features of silica are not apparent, indicating

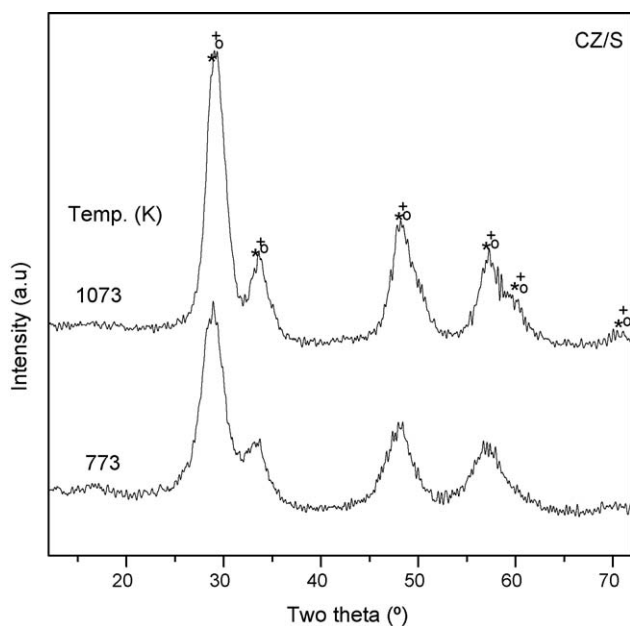


Fig. 1. Powder X-ray diffraction (XRD) patterns of $Ce_xZr_{1-x}O_2/SiO_2$ sample calcined at 773 and 1073 K. Peak legends are as follows: (*) lines due to $Ce_{0.75}Zr_{0.25}O_2$, (+) lines due to $Ce_{0.6}Zr_{0.4}O_2$ and (O) lines due to $Ce_{0.5}Zr_{0.5}O_2$.

the amorphous nature of the support. Though the formation of mixed phases between ceria–silica and zirconia–silica namely, $Ce_{9.33}(SiO_2)_6O_2$ and $ZrSiO_4$, respectively, are well-established in the literature [19,20], no such phases were noted in the present investigation. This observation clearly reveals the suitability of silica as an inert support for the dispersion of ceria–zirconia solid solutions. The non-appearance of these mixed compounds could be attributed to an intimate interaction between the Ce- and Zr-oxides leading to the formation of solid solutions and the inert character of the colloidal silica. The average crystallite size of Ce–Zr-oxides in the CZ/S sample, as a function of calcination temperature is summarized in Table 1. With increase in calcination temperature a small increase in the average crystallite size is noted. This observation clearly signifies the remarkable ability of silica to prevent agglomeration of $Ce_xZr_{1-x}O_2$ to form bigger crystallites. Such an influence of silica is also reflected in the specific surface areas of these oxides. A high BET surface area of $112\text{ m}^2\text{ g}^{-1}$ is retained even after the calcination at 1073 K (Table 1).

The TEM global picture along with HREM image and the corresponding selected area electron diffraction pattern (SAED) of the 773 K calcined sample is presented in Fig. 2. A closer view of the images reveals existence of small crystals of the size $\sim 5\text{ nm}$ dispersed over an amorphous silica matrix. The broad-

Table 1

BET surface area, average crystallite size and cell 'a' parameter measurements of cubic $Ce_xZr_{1-x}O_2$ in $Ce_xZr_{1-x}O_2/SiO_2$ catalysts calcined at 773 and 1073 K

Calcination temperature (K)	BET SA ($\text{m}^2\text{ g}^{-1}$)	Crystallite size ^a (nm)	Cell parameter 'a' values (Å)
773	172	3.1	5.35
1073	112	3.7	5.26

^a From XRD measurements.

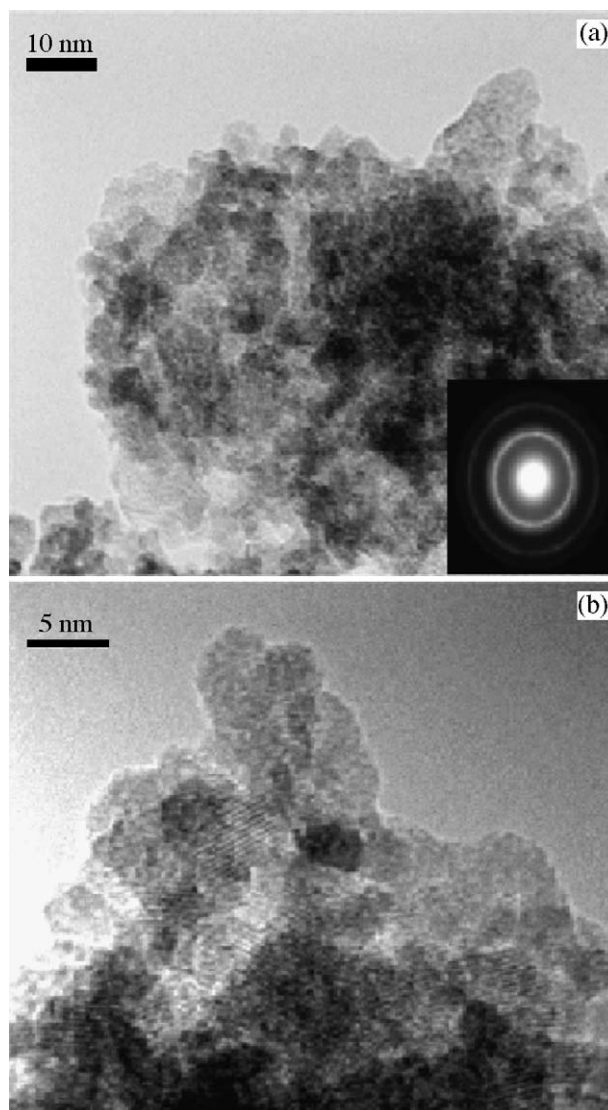


Fig. 2. (a) TEM and (b) HREM images of $Ce_xZr_{1-x}O_2/SiO_2$ sample calcined at 773 K.

ening of the rings in the electron diffraction patterns accounts for the presence of such small randomly oriented mixed oxide particles. The TEM and HREM images of the sample calcined at 1073 K are presented in Fig. 3, which reveal a well-dispersed, smaller Ce–Zr-oxide particles over the surface of the amorphous silica. Even after 1073 K calcination treatment, there was no apparent increase in the size of the Ce–Zr-oxide particles. These conclusions are drawn both from the observation of a few experimental images and the analysis of the selected area electron diffraction patterns. The fringes that appear in the micrograph allow for identification of the crystallographic spacings of the $Ce_xZr_{1-x}O_2$ nano-crystallites. Lattice fringes of around 3 Å were extensively observed on very small well-dispersed particles supported on the amorphous contrast for both the cases. The absence of additional electron diffraction rings pertaining to the tetragonal and monoclinic phases clearly indicates that the Ce–Zr-oxides are mainly in the cubic structure [16,21]. From the observation of experimental images and the analysis of the

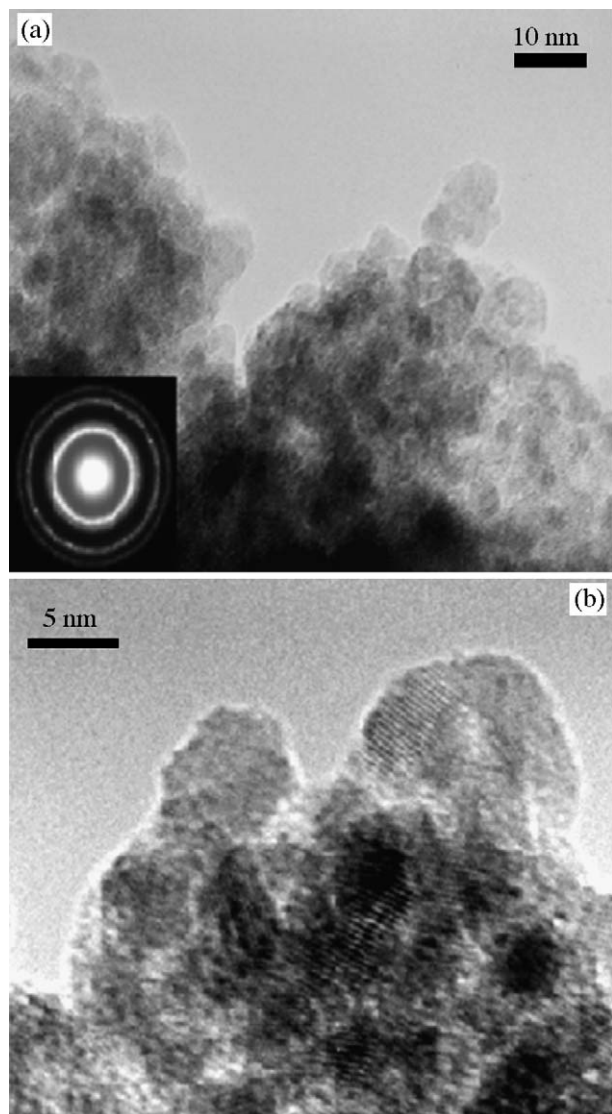


Fig. 3. (a) TEM and (b) HREM images of $Ce_xZr_{1-x}O_2/SiO_2$ sample calcined at 1073 K.

selected area electron diffraction patterns, it can be inferred that there was no apparent increase in the size of the Ce–Zr-oxide particles (~ 5 nm) up on increase of calcination temperature from 773 to 1073 K. Thus, the HREM results fairly support the observations made from XRD studies.

The $Ce_xZr_{1-x}O_2/SiO_2$ sample was further analysed by XPS technique to verify the elemental oxidation states. The electron binding energies of O 1s, Ce 3d, Zr 3d and Si 2p are presented in Table 2. Fig. 4 displays the Ce 3d spectra of the CZ/S sample

Table 2
Core level binding energy values for the $Ce_xZr_{1-x}O_2/SiO_2$ calcined at 773 and 1073 K

Calcination temperature (K)	Binding energy (eV)			
	O 1s	Ce 3d	Zr 3d	Si 2p
773	530.4	881.4	182.5	103.6
1073	530.1	881.1	182.4	103.4

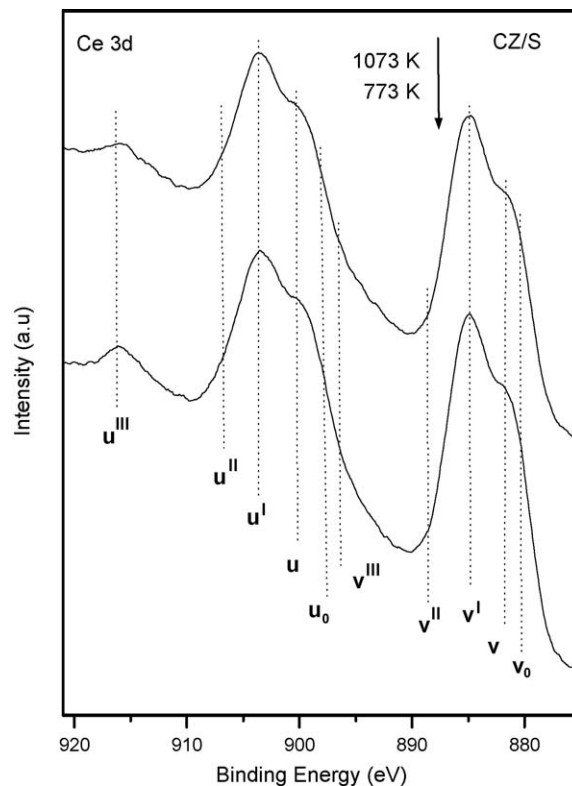


Fig. 4. Core level Ce 3d XP spectra of $Ce_xZr_{1-x}O_2/SiO_2$ sample calcined at 773 and 1073 K.

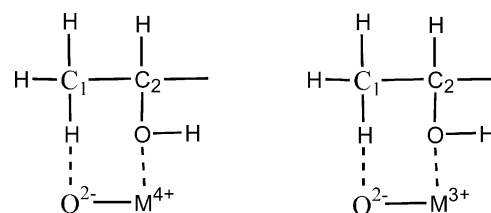
calcined at two different temperatures. The photoelectron peak shapes and the corresponding binding energies are sensitive to the calcination temperature. The binding energy values obtained for O 1s, Zr 3d and Si 2p are in agreement with the literature reports and clearly indicate the absence of pure ZrO_2 (182.9 eV) [17,22] and other inert compounds such as $CeSiO_4$ and $ZrSiO_4$ which can be identified with the Si 2p binding energy value at 101 eV [17,23]. The notation of Burroughs et al. [24] as envisaged in the literature, could be used to elucidate the Ce 3d peaks as shown in Fig. 4. Two sets of spin-orbital multiplets, corresponding to the $3d_{3/2}$ and $3d_{5/2}$ contributions were labeled as u and v, respectively. The peaks labeled v and v' have been assigned to a mixing of $Ce\ 3d^9\ 4f^2\ O\ 2p^4$ and $Ce\ 3d^9\ 4f^1\ O\ 2p^5$ Ce(IV) final states, and the peak denoted v'' corresponds to the $Ce\ 3d^9\ 4f^0\ O\ 2p^6$ Ce(IV) final state. Likewise, lines v_0 and v' are assigned to $Ce\ 3d^9\ 4f^2\ O\ 2p^5$ and $Ce\ 3d^9\ 4f^1\ O\ 2p^6$ of Ce(III). The same assignment could be applied to the u structures, which correspond to the Ce $3d_{3/2}$ levels. As the calcination temperature increases the intensity of the u''' peak decreased and intensity of the u' and v' annotated peaks increased, indicating an increase in the surface content of Ce^{3+} . However, the presence of Ce_2O_3 (Ce^{3+}) was not observed from the XRD measurements.

The dehydration of 4-methylpentan-2-ol may lead to different products and the composition of the product mixture depends on the mechanistic pathway of the reaction on the catalyst surface. This involves three types of mechanisms viz., concerted elimination pathway (E2), formation of carbocation (E1) and carbanion formation via two-point mechanism (E1cB) [22,23]. These mechanisms should be regarded as limiting cases, since inter-

mediate situations can occur. The carbanion route leads to the main product of terminal olefin (desired product) accompanied by the formation of small amount of ketones due to inevitable side reactions. On the other hand the operation of E1 mechanism (carbocation route) gives the undesired 2-ene as the main product with negligible amount of ketones. The concerted pathway (E2 mechanism) increases the yield of 2-ene in comparison to that of the desired terminal olefin, i.e. 4-methylpent-1-ene (Hofmann product). Cutrufello et al. and Solinas et al. [14,15] through their pioneering work have demonstrated that the E1cB route sets in for the case of ceria rich combinations in general, while zirconia rich combinations lead to mainly E2 path, thus resulting the desired and undesired products, respectively. Keeping these points in mind, the $Ce_xZr_{1-x}O_2/SiO_2$ composite catalyst mainly consisting of Ce rich phases, $Ce_{0.75}Zr_{0.25}O_2$ and $Ce_{0.6}Zr_{0.4}O_2$, were synthesized in the present investigation. The obtained product selectivity over the 773 K calcined catalyst as shown in Fig. 5, is in good agreement with the literature reports and obviously correlates well with earlier proposed concepts [25]. The selectivity of the desired product 4-methylpent-1-ene decreases from 85 to 57% with an increase in the reaction temperature from 533 to 673 K. The selectivity of 4-methylpentan-2-one increased from 6 to 28% indicating that at higher temperatures dehydration (side reaction of the E1cB) is more facile, which leads to the decrease in the selectivity of the desired product. However, the selectivity of 2-ene (Saytzeff product) does not show any appreciable change with increasing reaction temperature. This indicates that the E1 route (carbocation formation due to removal of hydroxyl group) does not gain more prominence revealing that the major reaction path could be carbanionic (E1cB).

One of the interesting observations from the present study is the lowering of reaction temperature at which 50% conversion occurs. The unsupported Ce–Zr mixed oxides with the combination of $Ce_{0.75}Zr_{0.25}O_2$ and $Ce_{0.5}Zr_{0.5}O_2$ phases having the

crystallite size of ~ 10 nm exhibited 50% conversion at a temperature of 633 K [23], while the silica stabilized Ce–Zr-oxides of below 5 nm (present study) indicate a temperature of 545 K for the same conversion with slightly better product distribution, which is intriguing. The decrease of temperature corresponding to 50% conversion could be attributed to the reduced crystallite size of the Ce–Zr-oxides, which exhibit increased reactivity due to very small size. An important clue has been observed from the XPS study, which reveals the presence of a significant amount of Ce^{3+} . The presence of Ce^{3+} may lead to an increase in the ability of the O^{2-} oxide ions to abstract a proton in comparison to O^{2-} oxide ions connected to Ce^{4+} and hence a carbanionic route (E1cB) could be facilitated as depicted below:



where $M^{4+} = Ce^{4+}$ or Zr^{4+} ; $M^{3+} = Ce^{3+}$.

As presented in Fig. 6, the $Ce_xZr_{1-x}O_2/SiO_2$ composite catalyst shows excellent performance in the time-on-stream experiments revealing the stable catalytic activity without deactivation. Recent literature reveals that ceria-based mixed oxides, especially ceria–zirconia combinations are highly coke resistant and exhibit promising stable activity without deactivation during time-on-stream runs for various reactions [9–11,26]. This was mainly attributed to the availability of lattice oxygen due to oxygen storage and release property of the Ce–Zr-oxides [14,26]. Thus, the present study indicates that amorphous silica can be used as an inert support to stabilize the Ce–Zr-oxide nano-sized crystallites against sintering at elevated temperatures that leads to a remarkable increase in the reactivity. Understanding com-

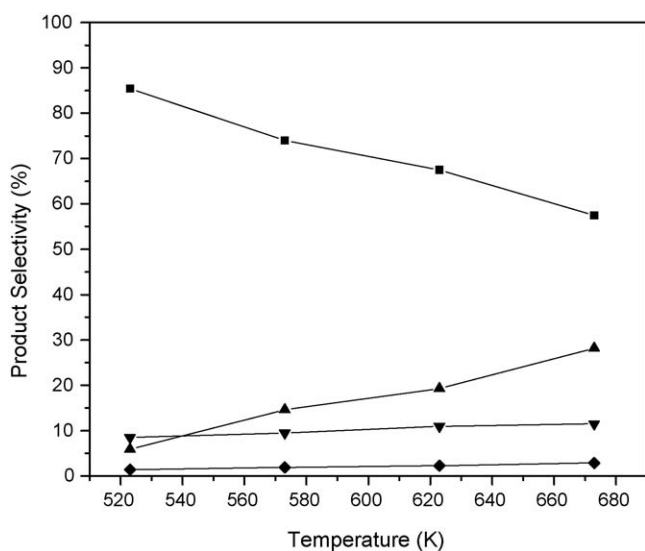


Fig. 5. Product selectivity vs. reaction temperature for the conversion of 4-methylpentan-2-ol over $Ce_xZr_{1-x}O_2/SiO_2$ catalyst: (■) 4-methylpent-1-ene, (▲) 4-methylpentan-2-one, (▼) 4-methylpent-2-ene and (◆) high molecular weight ketones.

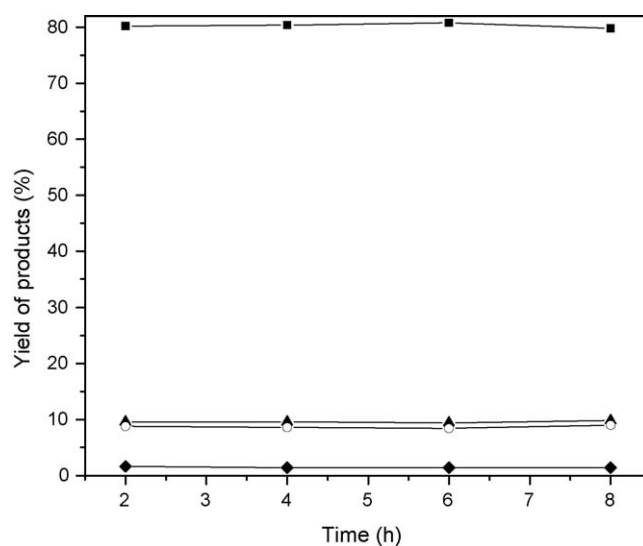


Fig. 6. Product yield vs. time-on-stream for the conversion of 4-methylpentan-2-ol over $Ce_xZr_{1-x}O_2/SiO_2$ catalyst at 541 K (50% conversion): (■) 4-methylpent-1-ene, (▲) 4-methylpentan-2-one, (○) 4-methylpent-2-ene and (◆) high molecular weight ketones.

plete structural features of the synthesized catalysts still remains difficult owing to very limited available literature and complexity arising due to the inherent heterogeneity of such systems. Hence further in-depth investigations on the local structure, directed towards improvement of the yield and selectivity are in active progress.

4. Conclusions

Surface stabilized nano-crystalline solid solutions of ceria–zirconia over silica support have been synthesized by a soft chemical route and were examined by various techniques after calcination at 773 and 1073 K. XRD measurements revealed the presence of $\text{Ce}_{0.75}\text{Zr}_{0.25}\text{O}_2$ at 773 K and $\text{Ce}_{0.6}\text{Zr}_{0.4}\text{O}_2$ and $\text{Ce}_{0.5}\text{Zr}_{0.5}\text{O}_2$ phases at 1073 K indicating more incorporation of zirconium into the ceria lattice at higher calcination temperature. HREM results indicated a well-dispersed nano-sized Ce–Zr-oxides (~5 nm) over the surface of amorphous silica. Particularly, the crystallite size does not show appreciable increase with increase of calcination temperature from 773 to 1073 K. XRD and HREM analysis further revealed the absence of ZrO_2 , CeSiO_4 , ZrSiO_4 and $\text{Ce}_{9.33}(\text{SiO}_2)_6\text{O}_2$ in the prepared $\text{Ce}_x\text{Zr}_{1-x}\text{O}_2/\text{SiO}_2$ nano-composite catalyst, throwing light on the superiority of the deposition precipitation technique adopted and the advantage of the colloidal silica being employed in this study. XPS study indicated the presence of appreciable amount of Ce^{3+} in the catalyst at both calcination temperatures. The highly stabilized and nano-crystalline $\text{Ce}_x\text{Zr}_{1-x}\text{O}_2/\text{SiO}_2$ composite catalyst exhibited a high activity for the conversion of 4-methylpentan-2-ol to 4-methylpent-1-ene and showed stable catalytic performance during the time-on-stream runs without deactivation. Also a significant fall in the reaction temperature corresponding to 50% conversion was observed over this composite catalyst.

Acknowledgments

We thank Dr. Y. Yamada, AIST-Osaka, Japan and Dr. A. Fernández, CSIC-UNSE-Sevilla, Spain for providing XPS and HREM results, respectively. P.L. thanks CSIR, New Delhi for senior research fellowship, and P.B. and P.S. thank CSIR, New Delhi for junior research fellowships. Financial support received from Department of Science and Technology, New Delhi under SERC Scheme (SR/S1/PC-31/2004).

References

- [1] H.S. Gandhi, G.W. Graham, R.W. McCabe, *J. Catal.* 216 (2003) 433.
- [2] A. Trovarelli, C. de Leitenburg, G. Dolcetti, *Chemtech* 27 (1997) 321.
- [3] S.J. Schmiege, D.N. Belton, *Appl. Catal. B: Environ.* 6 (1995) 127.
- [4] A. Trovarelli, M. Boaro, E. Rocchini, C. de Leitenburg, G.J. Dolcetti, *J. Alloys Comp.* 323 (2001) 584.
- [5] R. Si, Y.W. Zhang, S.J. Li, B.X. Lin, C.H. Yan, *J. Phys. Chem. B* 108 (2004) 2481, and the references therein.
- [6] R. Di Monte, J. Kaspar, *J. Mater. Chem.* 15 (2005) 633, and the references therein.
- [7] M. Daturi, E. Finocchio, C. Binet, J.C. Lavalley, F. Fally, V.J. Perrichon, *J. Phys. Chem. B* 103 (1999) 4884.
- [8] C. Bozo, F. Gaillard, N. Guilhaume, *Appl. Catal. A: Gen.* 220 (2001) 69.
- [9] S. Xu, X. Wang, *Fuel* 84 (2005) 563.
- [10] H.S. Roh, H.S. Potdar, K.W. Jun, *Catal. Today* 93–95 (2004) 39.
- [11] S. Larrondo, M.A. Vidal, B. Irigoyen, A.F. Craievich, D.G. Lamas, I.O. Fábregas, G.E. Lascalea, N.E. Walsøe de Reca, N. Amadeo, *Catal. Today* 107 (2005) 53.
- [12] D. Srinivas, C.V.V. Satyanarayana, H.S. Potdar, P. Ratnasamy, *Appl. Catal. A: Gen.* 246 (2003) 323.
- [13] K.B. Yi, E.J. Podlaha, D.P. Harrison, *Ind. Eng. Chem. Res.* 44 (2005) 7086.
- [14] M.G. Cutrufello, I. Ferino, V. Solinas, A. Primavera, A. Trovarelli, A. Auroux, C. Picciau, *Phys. Chem. Chem. Phys.* 1 (1999) 3369.
- [15] V. Solinas, E. Rombi, I. Ferino, M.G. Cutrufello, G. Colón, J.A. Navio, *J. Mol. Catal. A: Chem.* 204–205 (2003) 629.
- [16] G. Colon, M. Pijolat, F. Valdivieso, H. Vidal, J. Kaspar, E. Finocchio, M. Daturi, C. Binet, J.C. Lavalley, R.T. Baker, S. Bernal, *J. Chem. Soc. Faraday Trans.* 94 (1998) 3717.
- [17] D. Briggs, M.P. Seah (Eds.), *Practical Surface Analysis*, 2nd ed., Auger and X-ray Photoelectron Spectroscopy, vol. 1, Wiley, New York, 1990.
- [18] B.M. Reddy, I. Ganesh, *J. Mol. Catal. A: Chem.* 169 (2001) 207.
- [19] E. Rocchini, A. Trovarelli, J. Llorca, G.W. Graham, W.H. Weber, M. Maciejewski, A. Baiker, *J. Catal.* 194 (2000) 461.
- [20] B. Kucharczyk, W. Tylus, L. Kepinski, *Appl. Catal. B: Environ.* 49 (2004) 27.
- [21] B.M. Reddy, A. Khan, Y. Yamada, T. Kobayashi, S. Loidant, J.C. Volta, *J. Phys. Chem. B* 107 (2003) 11475.
- [22] P.C. Wong, Y.S. Li, K.A.R. Mitchell, *Surf. Rev. Lett.* 2 (1995) 297.
- [23] H. Behner, J. Wecker, T. Mathee, K. Samwer, *Surf. Interface Anal.* 18 (1992) 685.
- [24] A. Burroughs, A. Hamnett, A.F. Orchard, G.J. Thornton, *J. Chem. Soc. Dalton Trans.* 1 (1976) 1686.
- [25] D. Ciuparu, L. Pfefferle, *Catal. Today* 77 (2002) 167.
- [26] B.M. Reddy, P. Lakshmanan, S. Loidant, Y. Yamada, T. Kobayashi, C.L. Cartes, T.C. Rojas, A. Fernández, *J. Phys. Chem. B* 110 (2006) 9140.